



Subannual-to-biannual-resolved travertine record of Asian Summer Monsoon dynamics in the early Holocene at the eastern margin of Tibetan Plateau

Hailong Sun ^{a,b,*}, Chuan-Chou Shen ^{b,c}, Chung-Che Wu ^d, Bo Chen ^{a,e}, Jianjun Yin ^f, Hao Yan ^{a,g}, Jinguo Dong ^h, Dejun An ⁱ, Shu Tang ⁱ, Qingming Zhang ⁱ

^a State Key Laboratory of Environmental Geochemistry, Institute of Geochemistry, Chinese Academy of Sciences, Guiyang, 550081, China

^b High-Precision Mass Spectrometry and Environment Change Laboratory (HISPEC), Department of Geosciences, National Taiwan University, Taipei, 10617, Taiwan

^c Research Center for Future Earth, National Taiwan University, Taipei, 10617, Taiwan

^d Laboratory of Inorganic Chemistry, Department of Chemistry and Applied Biosciences, ETH Zurich, Zurich, 8093, Switzerland

^e College of Public Management, Guizhou University of Finance and Economics, Guiyang, 550025, China

^f Key Laboratory of Karst Dynamics, MNR and Guangxi, Guilin, Guangxi, 541004, China

^g International Center for Isotope Effects Research, School of Earth Sciences and Engineering, Nanjing University, Nanjing, 210023, China

^h College of Geosciences, Nantong University, Nantong, 226007, China

ⁱ Huanglong National Scenic Spot Administration, Songpan, 623300, China

ARTICLE INFO

Editorial handling: Prof. M. Kersten

Keywords:

Travertine
Asian summer monsoon
Oxygen isotope
Solar activity
Freshwater outburst
Early Holocene

ABSTRACT

In this study, we present a subannual–biannual-resolved (0.9–2 years) ASM intensity record spanning from 11.6 to 10.0 ka BP (before 1950 AD) inferred from a ^{230}Th -dated travertine $\delta^{18}\text{O}$ record at Zhangjia Ravine on the eastern margin of the Tibetan Plateau. The ZJG-1 $\delta^{18}\text{O}$ sequence is characterized by high-frequency fluctuations at decadal to centennial scales. Fluctuating between -11.15% and -14.78% over the $\delta^{18}\text{O}$ sequence, the fluctuation range gradually decreased from 11.6 to 10.0 ka BP. There are several abrupt changes in the $\delta^{18}\text{O}$ sequence, which indicate that the ASM in the early Holocene was highly unstable. Comparison with marine records suggests that the Preboreal oscillation (PBO) event could be triggered by a freshwater outburst which led to/resulted in a sudden release of thousands of cubic kilometers of the meltwater to the North Atlantic Ocean. Furthermore, the climate oscillations during the PBO were associated with the complex interplay of solar activity and freshwater outburst, the freshwater outburst may amplify the effect of solar activity when it was in the minima. The rapid warming after the PBO event may be controlled by the common mechanism that induced the Dansgaard–Oeschger warming events during the last glacial period. The further pronounced increases of the travertine $\delta^{18}\text{O}$ values occurred at about 10.3 ka BP, coinciding roughly with Bond 7 event, also caused by the freshwater outburst and solar activity. This study is not only important to understand the primary driving force of the ASM intensity in the early Holocene, but also essential for evaluate the probability of abrupt climate changes in the future.

1. Introduction

The Asian Summer Monsoon (ASM), including the East Asian summer monsoon and the Indian summer monsoon, is a major source of water vapor and heat within the global climate system (An et al., 2000; Gupta et al., 2003, 2013). Variations of the ASM can result in severe drought and flooding, which play a key role in the current and future socio-economic development of affected regions. ASM intensity varies

across multiple timescales, and understanding the decadal–centennial scale abrupt variations of ASM intensity and the driving factors is critical to better understand the dynamics and forcing of ASM variability.

Many studies have shown that the decadal to millennial scale ASM variations in the Holocene were linked to North Atlantic climate and caused by several driving forces, such as changes in solar activity (Gupta et al., 2003, 2005, 2013; Hong et al., 2003; Dykoski et al., 2005; Wang et al., 2005; Cai et al., 2010, 2012, 2015; Cheng et al., 2011; Xu et al.,

* Corresponding author. State Key Laboratory of Environmental Geochemistry, Institute of Geochemistry, Chinese Academy of Sciences, Guiyang, 550081, China.
E-mail address: sunhailong@vip.gyig.ac.cn (H. Sun).

2015; Zhang et al., 2018), freshwater outbursts to the North Atlantic Ocean (Fleitmann et al., 2008; Cheng et al., 2011; Liu et al., 2018; Sun et al., 2019), and the Intertropical Convergence Zone migration (Haug et al., 2001; Fleitmann et al., 2003; Dong et al., 2010; Bird et al., 2014; Sun et al., 2017). However, it remains uncertain whether solar activity directly drives the ASM or whether it indirectly affects it through the North Atlantic climate, especially for abrupt changes observed at decadal to centennial timescales (Gupta et al., 2003, 2005, 2013; Cheng et al., 2011; Xu et al., 2015). Therefore, the primary driving force for abrupt ASM variations at decadal–centennial timescales still needs to be determined.

Recent studies show that the climate in the early Holocene was unstable and dynamic, and had several abrupt cold events (Fisher et al., 2002; Teller et al., 2002; Magny et al., 2007; Berner et al., 2010). The Preboreal oscillation (PBO) was the first notable short, cool climatic variation after the Younger Dryas (Björck et al., 1996). Subsequently, Bond et al. (1997) found a series of cold events which occurred at about 8.1 ka BP, 9.4 ka BP, 10.3 ka BP and 11.1 ka BP in the early Holocene, and named 5, 6, 7, 8, respectively. The Bond 8 cold event in the study of Bond et al. (1997) is in fact the PBO event. The rate of these abrupt cold events is comparable to the climate changes in the Anthropocene. Understanding the mechanisms of the abrupt climate changes is critical to understand the abrupt climate changes in the Anthropocene and separate natural climate changes from anthropogenic.

The Tibetan Plateau (TP) is the highest plateau in the world, with an average altitude of about 4500 m. The TP plays an important role in the global climate system as it acts as an elevated heat source and a topographic barrier to the Asian monsoon (Yeh et al., 1957; Luo and Yanai, 1984; Wu and Zhang 1998; Sato and Kimura, 2005; Park et al., 2012). Moreover, the TP is one of the most sensitive areas to respond to global climate change (Liu and Chen, 2000). Therefore, the TP is an ideal site for studying the dynamics of the ASM (Zhou et al., 2010; Zhao et al., 2011; Cai et al., 2012; Bird et al., 2014; Zeng et al., 2017; Wang et al., 2019).

In recent decades, various archives from the TP have been investigated and applied to interpret the dynamics of the ASM in the Holocene (Hong et al., 2003; Zhou et al., 2010; Zhao et al., 2011; Cai et al., 2012; Zhang et al., 2018). However, more continuous and high-resolution Holocene records are required to evaluate the regional climate variation, especially the dynamics of the ASM and its underlying driving forces. Travertine and tufa are chemical sedimentary deposits that are deposited from flowing water in open-air conditions (Liu et al., 1995; Pentecost, 1995; Ford and Pedley, 1996), and their sediment sequences could play an important role in providing high-resolution palaeoclimate information (Liu et al., 2006, 2010; Sun and Liu, 2010) because of their high precipitation rates (mm to cm/year) (Matsuoka et al., 2001; Liu et al., 2006; Kano et al., 2007; Lojen et al., 2009; Brasier et al., 2010). The climate information of the geochemical proxies (chiefly $\delta^{18}\text{O}$ and $\delta^{13}\text{C}$) in travertine and tufa and their controlling mechanisms have been systematically revealed in previous studies (Matsuoka et al., 2001; Hori et al., 2008; Sun and Liu, 2010; Yan et al., 2012; Wang et al., 2014), providing a scientific foundation by which to accurately reconstruct palaeoclimate.

In this study, we present a high-resolution, absolutely dated and continuous travertine $\delta^{18}\text{O}$ record from Zhangjia Ravine on the eastern margin of the TP, China, and apply this to reconstructing the history of ASM intensity in this region. By comparing this record with North Atlantic climate records from Greenland ice core records, the marine sediment record from the Cariaco Basin, and ASM records from Indian and Chinese stalagmite records, we attempt to clarify the primary driving force of the monsoon intensity and the dominant force of the abrupt changes in ASM intensity at decadal to centennial timescales. These results are not only important to understand the abrupt climate changes in the early Holocene but also essential for understanding the unstable climate conditions during the early Holocene, and the abrupt climate changes in the Anthropocene.

2. Site and sample description

Zhangjia Ravine ($103^{\circ}52'\text{E}$, $32^{\circ}34'\text{N}$) is located in the east Huanglong scenic area on the eastern margin of the TP; it is 230 km NW of the provincial capital of Sichuan Province, Chengdu (Fig. 1). It is 5 km in length and 20–50 m in width, with a high-elevation mountainous climate. The geology consists of Paleozoic carbonate rocks exceeding 4000 m in thickness, overlain by about 1000 m of Mesozoic clastic rocks, Cenozoic alluvial gravels, glacial moraines, and travertine (Liu et al., 1995). This region lies at the convergence zone of the Indian monsoon and East Asian monsoon, with most of the rainfall in the region is a direct result of the warm and wet air from the Indian and Pacific Oceans (Hong et al., 2003; Yang et al., 2007; Zhou et al., 2010). This region is not only sensitive to the monsoon changes, but also sensitive to direct insolation heating because of its high altitude (>3000 m above sea level). The average annual precipitation at Huanglong is 759 mm and the mean air temperature is 1.1°C . About 72% of the annual precipitation occurs during the rainy ASM season from May to September (Wang et al., 2014).

The travertine profile ZJG-1 examined in this study was outcropped at the upper reaches of Zhangjia Ravine, about 3599 m above sea level, and is about 5.5 m in height and 10 m in width (Fig. 2a). This profile is endogenous (thermogenic) travertine, from which the carbon dioxide is sourced from a range of situations including hydrolysis and oxidation of reduced carbon, decarbonation of limestone or directly from the upper mantle (Pentecost, 1995; Ford and Pedley, 1996; Liu et al., 2003; Wang et al., 2010, 2014). The surface is characterized by a dark brown color due to thousands of years of weathering. The carbonate under the weathered layer has a clear lamination structure, consisting of alternating thin dark layers and thick dense layers (Fig. 2b). The dark color of the thin porous layers is attributed to soil-derived clay and organic matter introduced by overland flow (Liu et al., 2010).

3. Methods

Samples for stable isotope analysis were collected by the following method: 1) Removing the upper 20–30 cm of the weathered layer, and the remaining pristine travertine was cut into different size blocks (5–10 cm long) from the profile using a diamond saw in the field. 2) Subsamples, 100–500 μg each, were milled using dental drill bits ranging in size from 0.5 to 1 mm directly from the polished surface of the blocks, and the spacing between subsamples ranged from 0.1 to 2 cm.

The oxygen stable isotopic compositions of 1236 subsamples were analyzed on a Finnigan MAT-253 mass spectrometer linked to an on-line automated preparation system (Thermo-Fisher GasBench II) at the State Key Laboratory of Environmental Geochemistry, Guiyang, China. The international standard NBS-19 and three Chinese standards (GBW04405, GBW04406, and GBW04416) were measured every 15–20 subsamples, with an external 1-sigma precision of $\pm 0.1\text{\textperthousand}$. Isotopic data are reported relative to Vienna Pee Dee Belemnite (VPDB).

Powdered subsamples for U-Th dating were drilled from seven layers on the polished surface of the blocks on a class-100 laminar flow bench in a class-10,000 subsampling room to avoid possible contamination (Shen et al., 2003, 2012). For the two layers at 356 cm (ZJG1-3-221) and 435 cm (ZJG1-3-156), four coeval subsamples were drilled, and three coeval subsamples were drilled at 623 cm (ZJG1-2-1). U-Th isotopic compositions and concentrations were determined by a Thermo-Fisher NEPTUNE multi-collection inductively coupled plasma mass spectrometer (MC-ICP-MS) at the High-Precision Mass Spectrometry and Environment Change Laboratory (HISPEC), Department of Geosciences, National Taiwan University (Shen et al., 2012). Detailed methods of U-Th chemistry, instrumental analysis, and age calculation are described in Shen et al. (2002), Shen et al. (2012), and Cheng et al. (2013), respectively. All date errors given are two standard deviations unless otherwise noted.

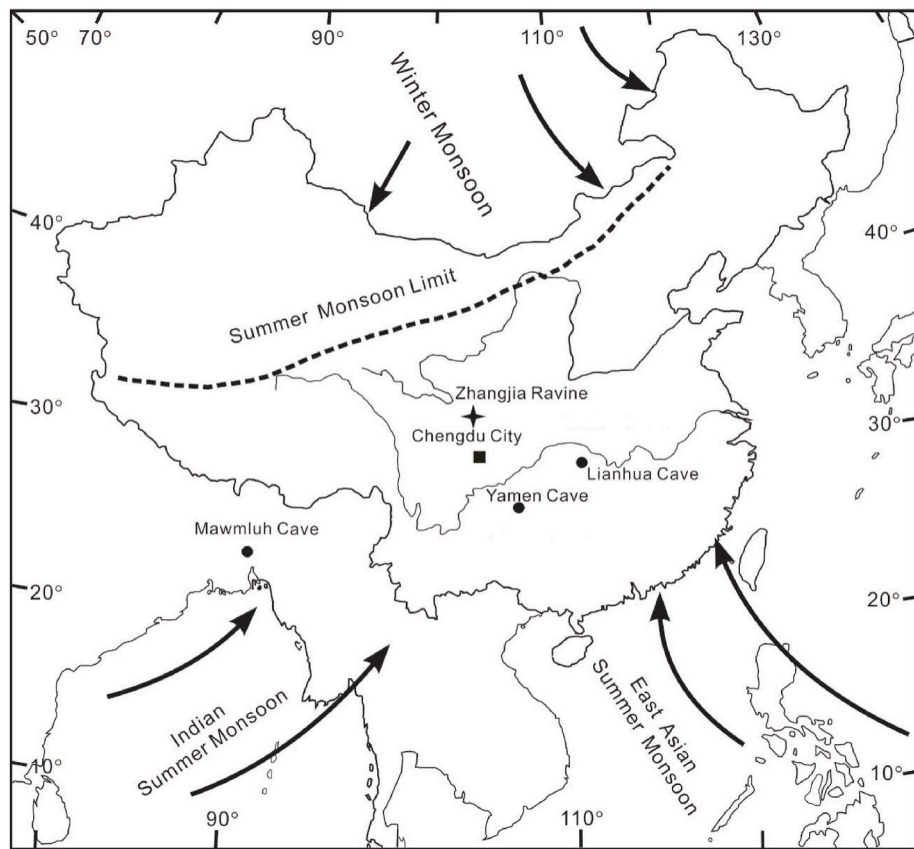


Fig. 1. Location of the Zhangjia Ravine, Yamen Cave (Yang et al., 2010), Mawmluh Cave (Berkelhammer et al., 2012), Lianhua Cave (Zhang et al., 2016) and the current monsoonal climatic system in China, including the East Asian and Indian Summer Monsoons, and the winter monsoon. The summer monsoon is a steady flow of warm, moist air from the tropical oceans, and the winter monsoon is a flow of cold, dry air associated with the Siberian-Mongolian High. The dashed lines represent the approximate summer monsoon limit at present.

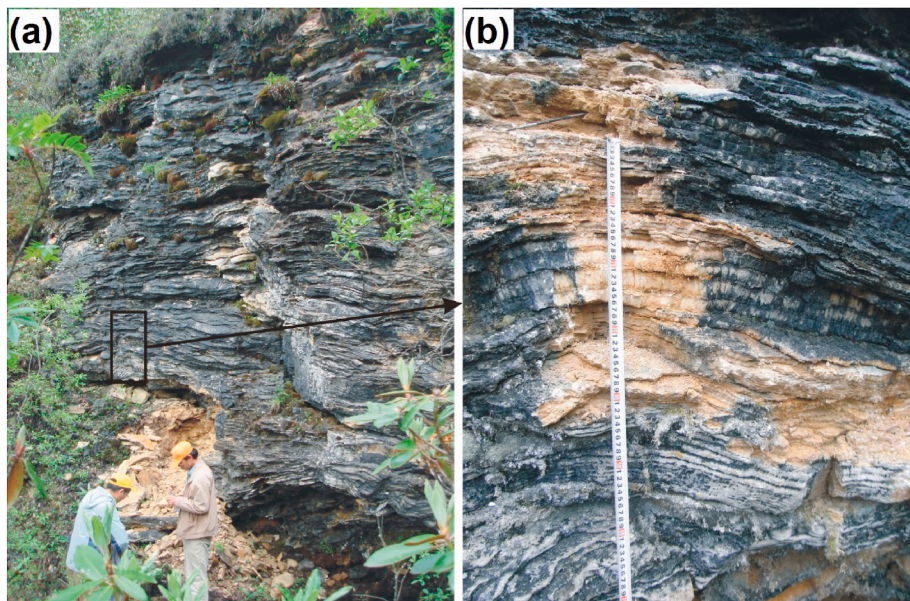


Fig. 2. Photographs of (a) the whole travertine profile of the studied travertine profile ZJG-1 and (b) the annually laminated structure of travertine deposits at Zhangjia Ravine.

4. Results

4.1. ^{230}Th dates and age model

U-Th dating results are given in Table 1. Concentrations range between 346 and 588 ppb for ^{238}U . Uncertainty of corrected ^{230}Th dates ranges from ± 39 to ± 881 yr. All ^{230}Th ages are in stratigraphic order

within the range of errors. The age-depth model was established using the COPRA algorithm (Breitenbach et al., 2012, Fig. 3). The age model shows that the deposition interval is from 11.6 to 9.0 thousand years ago (ka BP, before 1950 AD). The calculated deposition rate of the travertine profile varied from ~ 0.9 mm/year to ~ 6.1 mm/year (Fig. 3).

Table 1U-Th isotopic compositions and ^{230}Th dates for travertine profile ZJG-1 by MC-ICP-MS techniques at HISPEC, NTU.

Sample number	Depth (cm)	^{238}U (ppb)	^{232}Th (ppt)	$\delta^{234}\text{U}$ (measured)	$\delta^{234}\text{U}_{\text{initial}}(\text{corrected})$	$^{230}\text{Th}/^{238}\text{U}$ (activity)	$^{230}\text{Th}/^{232}\text{Th}$ (ppm)	Age (yr) (uncorrected)	Age (yr) (corrected)
ZJG1-4-1	40	345.73 ± 0.28	36555 ± 196	626.7 ± 1.5	643.0 ± 2.2	0.1543 ± 0.0024	24.07 ± 0.39	10,741 ± 172	9,027 ± 881
ZJG1-3-401	104	420.91 ± 0.56	3740 ± 10	640.3 ± 2.6	658.3 ± 2.6	0.14401 ± 0.00090	267.3 ± 1.8	9,900 ± 67	9,758 ± 98
ZJG1-3-338	211	408.48 ± 0.61	2672.5 ± 9.0	646.9 ± 2.9	665.6 ± 3.0	0.14741 ± 0.00093	371.5 ± 2.6	10,102 ± 70	9,998 ± 87
ZJG1-3-274	296	587.83 ± 0.54	12511 ± 44	672.6 ± 1.6	650.5 ± 4.5	0.1575 ± 0.0013	122.0 ± 1.1	10,719 ± 95	10,319 ± 192
ZJG1-3-221a	351	557.5 ± 1.2	7128 ± 37	671.2 ± 4.6	691.8 ± 4.8	0.1600 ± 0.0012	206.6 ± 1.8	10,863 ± 90	10,663 ± 135
ZJG1-3-221b	351	545.80 ± 0.89	5803 ± 26	673.0 ± 3.7	693.7 ± 3.8	0.1597 ± 0.0011	248.0 ± 2.0	10,826 ± 82	10,660 ± 117
ZJG1-3-221c	351	521.8 ± 1.9	6731 ± 35	665.1 ± 7.6	685.6 ± 7.9	0.1592 ± 0.0018	203.7 ± 2.4	10,841 ± 139	10,638 ± 171
ZJG1-3-221d	351	534.9 ± 1.1	5026 ± 16	671.6 ± 4.2	692.3 ± 4.3	0.15940 ± 0.00095	280.1 ± 1.8	10,814 ± 73	10,667 ± 104
								Wt-averaged date*	10,660 ± 63
ZJG1-3-156a	436	387.15 ± 0.64	3443 ± 11	668.5 ± 3.4	690.2 ± 3.5	0.16790 ± 0.00070	311.3 ± 1.6	11,424 ± 56	11,285 ± 89
ZJG1-3-156b	436	364.34 ± 0.55	2710 ± 10	672.6 ± 2.8	694.5 ± 2.9	0.16793 ± 0.00073	372.2 ± 2.0	11,396 ± 56	11,280 ± 81
ZJG1-3-156c	436	394.98 ± 0.70	3869 ± 14	672.8 ± 3.6	694.6 ± 3.7	0.16823 ± 0.00081	283.2 ± 1.6	11,417 ± 64	11,264 ± 99
ZJG1-3-156d	436	376.63 ± 0.71	4125 ± 16	673.1 ± 3.5	694.9 ± 3.7	0.16829 ± 0.00093	253.3 ± 1.7	11,418 ± 71	11,247 ± 111
								Wt-averaged date*	11,272 ± 47
ZJG1-2-1a	623	474.45 ± 0.56	1914.5 ± 7.0	670.5 ± 2.0	692.9 ± 2.0	0.17141 ± 0.00051	700.4 ± 3.2	11,661 ± 40	11,598 ± 51
ZJG1-2-1b	623	439.49 ± 0.56	5129 ± 13	670.4 ± 1.7	692.7 ± 1.8	0.1728 ± 0.0010	244.1 ± 1.5	11,759 ± 73	11,577 ± 117
ZJG1-2-1c	623	396.06 ± 0.63	2516.4 ± 8.4	668.2 ± 2.7	690.5 ± 2.8	0.17087 ± 0.00065	443.4 ± 2.1	11,640 ± 51	11,540 ± 71
								Wt-averaged date*	11,578 ± 39

Analytical errors are 2σ of the mean. Decay constant values are $\lambda_{230} = 9.1705 \times 10^{-6} \text{ yr}^{-1}$, $\lambda_{234} = 2.8221 \times 10^{-6} \text{ yr}^{-1}$ (Cheng et al., 2013) and $\lambda_{238} = 1.55125 \times 10^{-10} \text{ yr}^{-1}$ (Jaffey et al., 1971). Corrected ^{230}Th age calculation is based on an assumed initial $^{230}\text{Th}/^{232}\text{Th}$ atomic ratio of $(4 \pm 2) \times 10^{-6}$. All corrected dates are relative to 1950.

**The formula for averaged uncertainty is $\left(\frac{1}{\sum \left(\frac{1}{(\text{Error})^2} \right)} \right)^{0.5}$, where Error is the uncertainty of ^{230}Th date. The weighted date is calculated with a formula of

$\left(\frac{\sum \text{Age} / (\text{Error})^2}{\sum \left(\frac{1}{(\text{Error})^2} \right)} \right)^{0.5}$, where Age is the determined ^{230}Th date."

4.2. Oxygen isotope records

The sampling strategy of the travertine profile yielded a temporal resolution of 0.9–2 years (an average resolution of 1.3 years). The travertine profile ZJG-1 $\delta^{18}\text{O}$ shows several distinct features (Fig. 4). The ZJG-1 $\delta^{18}\text{O}$ sequence is characterized by high-frequency fluctuations at decadal to centennial scales. Fluctuating between $-11.15\text{\textperthousand}$ and $-14.78\text{\textperthousand}$ over the $\delta^{18}\text{O}$ sequence, with an average of $-13.20\text{\textperthousand}$, and the fluctuation range gradually decreased from 11.6 to 10.0 ka BP. The $\delta^{18}\text{O}$ values fluctuated in a large range at the centennial scale, and frequent, abrupt decadal-scale shifts in the $\delta^{18}\text{O}$ values are superimposed on these centennial scale changes. The fluctuation range of $\delta^{18}\text{O}$ values in the ZJG-1 profile is about $3.63\text{\textperthousand}$. There are several large abrupt changes in the $\delta^{18}\text{O}$ sequence. One occurred at about 11.3 ka BP, when the $\delta^{18}\text{O}$ value increased from $-14.78\text{\textperthousand}$ at 11.44 ka BP to the highest value of $-11.47\text{\textperthousand}$ at 11.32 ka BP, with a range of $3.31\text{\textperthousand}$. This rapid change covers about 120 years. The second major abrupt change in the $\delta^{18}\text{O}$ sequence can be observed between 11.32 and 11.25 ka BP, followed by a rapid $\delta^{18}\text{O}$ decrease of $3.15\text{\textperthousand}$ (from $-11.47\text{\textperthousand}$ to $-14.62\text{\textperthousand}$). This rapid change covers about 70 years. From 10.9 to 10.0 ka BP, the variation range of $\delta^{18}\text{O}$ is relatively small, and the $\delta^{18}\text{O}$ value decreased overall, indicating that the ASM strengthened gradually. However, several

abrupt increases in $\delta^{18}\text{O}$ values occurred at about 10.65 and 10.3 ka BP. The increase in $\delta^{18}\text{O}$ values occurring at about 10.3 ka BP coincides roughly with the Bond 7 event (Bond et al., 1997, 2001).

5. Discussions

5.1. Interpretation of $\delta^{18}\text{O}$ in the travertine calcite

Before interpreting travertine $\delta^{18}\text{O}$ as a climatic proxy, it is important to understand its climatic implications and climatic controlling mechanisms. Wang et al. (2014) found that the $\delta^{18}\text{O}$ values of travertine deposited in the ramp stream in Huanglong area were low in the warm rainy season and high in the cold dry season. The low $\delta^{18}\text{O}$ values of travertine were caused by the low $\delta^{18}\text{O}$ values in water induced by seasonal variation in oxygen isotopic ratios of precipitation (lower in summer and higher in winter). Therefore, the $\delta^{18}\text{O}$ present in the travertine records the $\delta^{18}\text{O}$ values of the precipitation. In low-latitude areas, the rainwater $\delta^{18}\text{O}$ values have a negative correlation with rainfall amount, which is known as the “rainfall amount effect”. It has been indicated that rainfall amount is the major controlling factor of rainwater $\delta^{18}\text{O}$ (Dansgaard, 1964; Rozanski et al., 1992). Therefore, the variations of travertine $\delta^{18}\text{O}$ at Zhangjia Ravine reflect the variations of

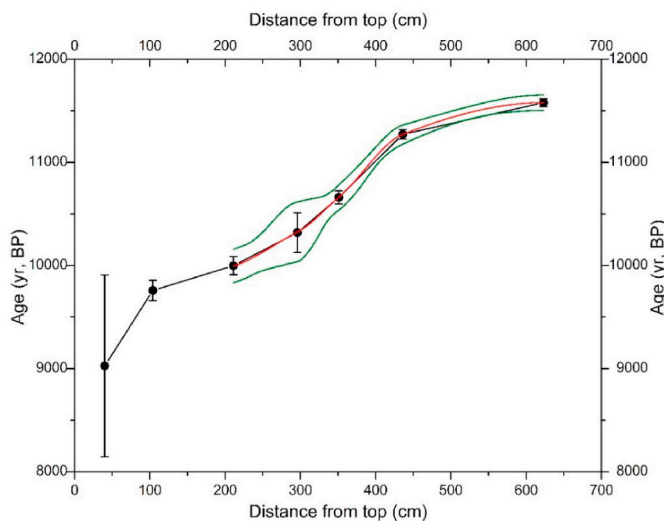


Fig. 3. Map showing Age versus depth for the travertine profile ZJG-1. All ages are reported as thousand years before the present (ka BP; 1950 AD). The age errors indicated in the plots are 2σ error.

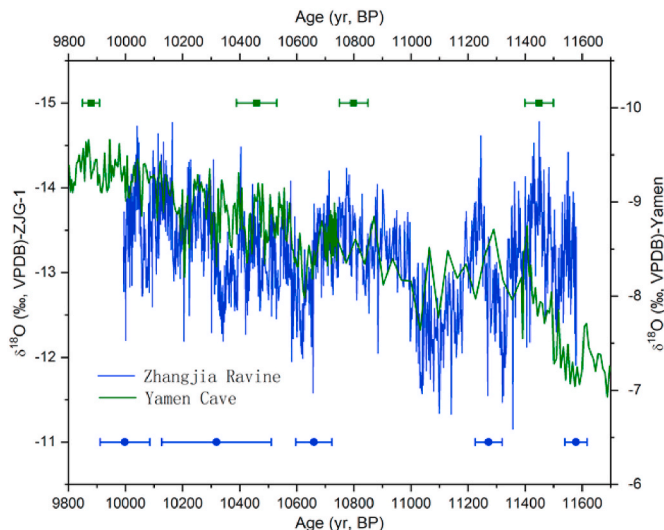


Fig. 4. $\delta^{18}\text{O}$ time series of travertine profile ZJG-1 (blue line) and the $\delta^{18}\text{O}$ time series of stalagmite Y1 from Yamen cave (Yang et al., 2010; green line).

rainfall amount, and the travertine $\delta^{18}\text{O}$ values can be considered an indicator of Monsoon intensity. The $\delta^{18}\text{O}$ values of travertine in the ramp system were also affected by water temperature and kinetic fractionation (Wang et al., 2014). In the calcite-water fractionation equation, $\delta^{18}\text{O}_w$ and the temperature play an equal role, so the temperature also played a major role in the $\delta^{18}\text{O}$ values of travertine (O'Neil et al., 1969). The kinetic effect is considered low because the travertine was deposited in the upper reaches where the kinetic effect is weaker (Yan et al., 2017).

The replication test is a powerful tool for evaluating whether the climate proxies of travertine or speleothem recorded the primary climate signals (Dorale and Liu, 2009). In the current study, the $\delta^{18}\text{O}$ records of the ZJG-1 travertine profile were compared with the speleothem $\delta^{18}\text{O}$ records from Yamen cave, which the stalagmite was absolutely dated and the $\delta^{18}\text{O}$ records synchronously vary with other speleothem records in Asian monsoon area (Yang et al., 2010). The ZJG-1 $\delta^{18}\text{O}$ record broadly follow the same variation trends of Yamen $\delta^{18}\text{O}$ record though their absolute $\delta^{18}\text{O}$ values are different (Fig. 4). This agreement indicates that changes in the $\delta^{18}\text{O}$ record of travertine are

mainly influenced by large-scale climate changes, rather than the kinetic fractionation.

Therefore, the ZJG-1 travertine $\delta^{18}\text{O}$ changes in this study can be interpreted as a reliable indicator of variations in ASM intensity as the variations in travertine $\delta^{18}\text{O}$ values reflect the intensity of the ASM in the region. It should be noted that the fluctuation range of the ZJG-1 $\delta^{18}\text{O}$ record is larger than the Yamen $\delta^{18}\text{O}$ record (Fig. 4). This may be attributed to the deposition environment of the travertine and the sensitivity of the high elevation of TP to climate change (Cai et al., 2012). The speleothem $\delta^{18}\text{O}$ values show a lower amplitude of variations because the deposition in the cave is less suspected to daily and seasonal variations, and of course, the water in the unsaturated zone feeding the cave is less variable compared with single rain event feeding the travertine (Ayalon et al., 1998; Orland et al., 2014; Sun and Liu, 2010). Travertine deposits in the surface and the parent water are directly influenced by climate and environment, including factors such as temperature and precipitation levels (Matsuoka et al., 2001; Kano et al., 2007; Liu et al., 2010; Sun and Liu, 2010). Therefore, the travertine $\delta^{18}\text{O}$ value is a highly sensitive proxy that can directly reflect the changes of precipitation $\delta^{18}\text{O}$ values and preserve the original climate information (Sun and Liu, 2010; Wang et al., 2014).

5.2. ASM intensity variations recorded by travertine $\delta^{18}\text{O}$ and their response to North Atlantic climate and solar activity

To better understand the primary driving force of the abrupt ASM variations in the early Holocene, we compare our record to those from other sites (Fig. 5). As shown in Fig. 5, the travertine $\delta^{18}\text{O}$ decreased overall from 11.6 to 10.0 ka BP, indicating the ASM intensity increased in the early Holocene. The travertine ZJG-1 $\delta^{18}\text{O}$ record synchronized well with those climate records from the Greenland ice cores, GISP2 (Stuiver et al., 1997) and NGRIP (Rasmussen et al., 2007); the titanium concentration data from the Cariaco Basin, the tropical Atlantic (Haug et al., 2001); the speleothem $\delta^{18}\text{O}$ record from Mawmluh cave in north India (Berkelhammer et al., 2012); and the speleothem record of Yamen cave (Yang et al., 2010), southwest China. The travertine $\delta^{18}\text{O}$ record is also generally consistent with reconstructions of the ASM from Lianhua cave (Zhang et al., 2016).

The similarity of the travertine $\delta^{18}\text{O}$ record from Zhangjia Ravine and the $\delta^{18}\text{O}$ record from Mawmluh Cave and Yamen Cave reflects the influence of the ASM on climatic conditions in the Huanglong area. The similarity of the spatially separated records reflects the large spatial extent of the ASM. The ASM intensity changes recorded in travertine $\delta^{18}\text{O}$ in phase with the North Atlantic climate confirm the close teleconnection between the ASM and the North Atlantic climate not only at millennial to centennial scales (Gupta et al., 2003; Hong et al., 2003; Wang et al., 2005) also at decadal scales during the early Holocene.

Solar activity appears to have played an important role in the abrupt climate changes in the Holocene (Björck et al., 1996; Nesje et al., 2004; van der Plicht et al., 2004; Magny et al., 2007). Fig. 6 shows the most striking feature of the travertine $\delta^{18}\text{O}$ record that is the close correlation between ASM intensity changes and sunspot number activity inferred from tree-ring $\Delta^{14}\text{C}$ data, which reflect the solar activity (Solanki et al., 2004, Fig. 6). Fig. 6 reveals that the ASM intensity changes (including the decadal to centennial scale changes) synchronize well with sunspot number activity; the increase in ASM intensity coincides with the increase in solar output and vice versa. The significant correlation between the ASM intensity and the solar activity indicates that the primary control of decadal to centennial scale variations in ASM intensity is solar activity, and small changes in solar activity can bring pronounced changes in ASM intensity. Furthermore, the synchronous changes between the ASM intensity changes and solar activity confirm that the ASM responds almost immediately to solar activity changes (Wang et al., 2005). Kodera (2004) suggested that the solar influence on monsoon activity originates from the stratosphere through a modulation of the upwelling in the equatorial troposphere, which produces a north-south

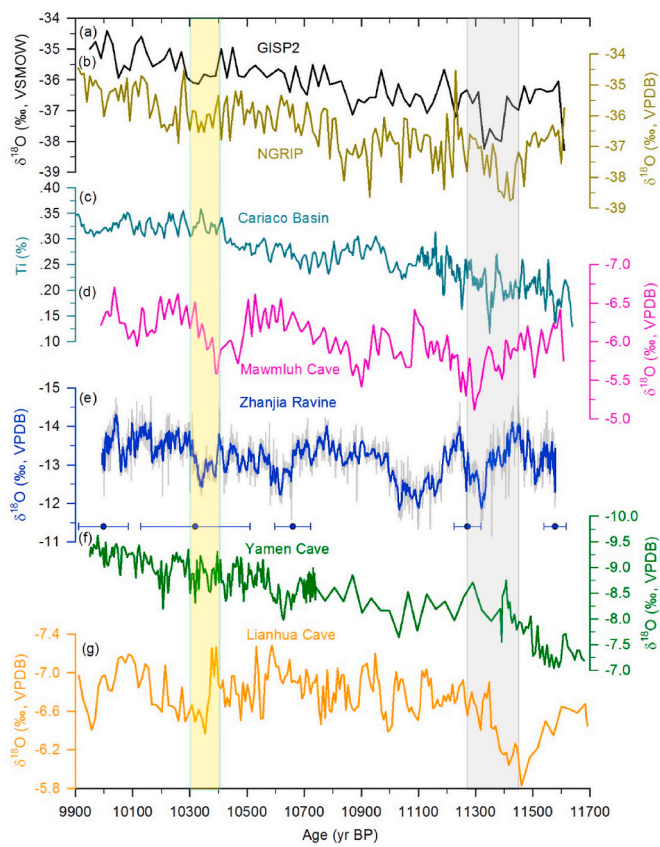


Fig. 5. Comparison of the travertine $\delta^{18}\text{O}$ record with records of North Atlantic climate and stalagmite records from south of China. (a) Oxygen isotopic record from the GISP2 ice core, Greenland (Stuiver et al., 1997). (b) Oxygen isotopic record from the NGRIP ice core, Greenland (Rasmussen et al., 2007). (c) Titanium concentration data from the Cariaco Basin, tropical Atlantic (Haug et al., 2001). (d) $\delta^{18}\text{O}$ record of the Mawmluh Cave stalagmite KM-A (Berkelhammer et al., 2012). (e) $\delta^{18}\text{O}$ record of the travertine profile ZJG-1 (the blue line is a 5-point running average). (f) $\delta^{18}\text{O}$ record of the Yamen Cave stalagmite Y1 (Yang et al., 2010). (g) $\delta^{18}\text{O}$ record of the Lianhua Cave stalagmite LHD5 (Zhang et al., 2016). The gray vertical bar illustrates the PBO event and the rapid warming event after the PBO event. The yellow vertical bar illustrates the Bond 7 event.

seesaw of convective activity in the Indian sector during summer. Increased solar activity would thus enhance the convective activity in the equatorial region and increase precipitation. Similar conclusions were drawn by Gupta et al. (2005), who reported the relationship between sunspot activity and the record of the Indian Summer Monsoon winds and revealed multiple intervals of weak summer monsoon during the Holocene at multi-decadal to centennial scales. Therefore, the variations in solar activity played a critical role in abrupt climate changes in the early Holocene.

5.3. Abrupt changes in ASM intensity in the early Holocene and their linkages with the combination of solar activity and freshwater outburst events

The ZJG-1 $\delta^{18}\text{O}$ variability in the whole sequence is characterized by high-frequency fluctuations at decadal to centennial scales, indicating highly unstable climate conditions in the early Holocene. Fig. 5 shows that the decadal to centennial scale abrupt changes in ASM intensity recorded in ZJG-1 $\delta^{18}\text{O}$ values can be identified and synchronize well with changes in other records (Section 5.2). For example, a pronounced abrupt increase of $\delta^{18}\text{O}$ values occurred at about 11.3 ka BP, with an amplitude of $\sim 3.63\text{\textperthousand}$ ($-14.78\text{\textperthousand}$ to $-11.15\text{\textperthousand}$, Fig. 6), which can be

identified as the PBO. A further pronounced increases of $\delta^{18}\text{O}$ values occurred at about 10.3 ka BP, which coincide roughly with Bond 7 event (Bond et al., 1997, 2001).

Apart from the variations in solar activity, the freshwater outburst has been considered as possible driving force for the abrupt climate changes in the early Holocene. Fisher et al. (2002) found that the origin of the PBO was associated with a large, but short lived, increase in freshwater outburst to the Arctic Ocean. They estimated that only 2%–4% of the floodwater would have frozen into sea ice within the Beaufort region, coupled with increased river ice production during winter, and thicker pack ice growth throughout the Arctic Ocean. The thicker and more extensive pack ice and freshened sea surface may have triggered the PBO by increasing albedo, generating a low-salinity anomaly upon melting in the North Atlantic and thus decreasing the formation of North Atlantic Deep Water (NADW). The decreased NADW formation may have weakened the Atlantic Meridional Overturning Circulation (AMOC) and induced the southward shift of the mean latitudinal position of the ITCZ (Fleitmann et al., 2007). Magny et al. (2007) found that the PBO was a response to successive freshwater outburst at 11.3, 11.25 and 11.17 ka BP and to a sudden decrease in solar activity. Bond et al. (1997) considered that the Bond 7 event was caused by reduced NADW production. The decreasing formation of NADW may be correlated to the freshwater outburst event around 10.3 ka BP (Teller et al., 2002).

In this study, two decadal sub-cycles of ASM oscillations can be observed during the PBO period, which coincide with variations in sunspot number (Fig. 6). This indicates the close association between decadal-scale climate changes and solar activity during the PBO. Fig. 6 shows that the solar activity reached a relatively high value at the onset of the PBO, then the solar activity had a sudden decline and ASM showed synchronous decrease until 11.33 ka BP when the solar activity reached the minima, and the freshwater outburst also occurred at this time (Fisher et al., 2002; Solanki et al., 2004). But the ASM continued to decrease and reached the lowest value at about 11.32 ka BP. These results suggest that the PBO was triggered by the freshwater outburst, which may be related to the relatively high solar activity. Correspondingly, the climate oscillations during the PBO were associated with the complex combination of solar activity and the freshwater outburst, and the freshwater outburst may amplify the effect of solar activity when the solar activity was in minima, and make the ASM variations lag the solar activity. This supports the suggestion of Bond et al. (2001) that solar activity may be the primary driving force of North Atlantic's Holocene climate, and the change in the North Atlantic deep water caused by the freshwater outburst may amplify the solar activity changes at decadal to centennial scales.

After the PBO, the ZJG-1 $\delta^{18}\text{O}$ rapidly decreased from $-11.47\text{\textperthousand}$ to $-14.62\text{\textperthousand}$ within about 70 years (from 11.32 ka BP to 11.25 ka BP), and the ASM intensity abruptly strengthened (Fig. 6). A similar abrupt warming after the PBO can be identified in the Greenland ice core GISP2 (Stuiver et al., 1997; Kobashi et al., 2008) and NGRIP (Rasmussen et al., 2007) data (Fig. 5). During this abrupt warming period, the variations of the sunspot number, which exhibited a decreasing trend, was inconsistent with changes in the ZJG-1 $\delta^{18}\text{O}$ sequence (Fig. 6). Therefore, solar activity was not the driving force of this abrupt climate change.

This rapid warming event after the PBO is similar to the abrupt Dansgaard–Oeschger (D-O) warming events in the last glacial period, during which the temperature increased by 5–10 °C within a few decades (Dansgaard et al., 1993). These two similar abrupt warming events could be induced by a common mechanism (Kobashi et al., 2008). There is strong evidence that the origin of D-O events is related to variations in the strength of the AMOC and its associated heat transport (van Kreveld et al., 2000; Ganopolski and Rahmstorf, 2001; Elliot et al., 2002; Clement and Peterson, 2008; Dokken et al., 2013). Ganopolski and Rahmstorf (2001) suggested that there is a “warm” circulation mode of the AMOC during the D-O events. The warm circulation mode is only marginally unstable, and temporary transitions to this warm mode can be easily triggered by minor freshwater perturbations, leading to an

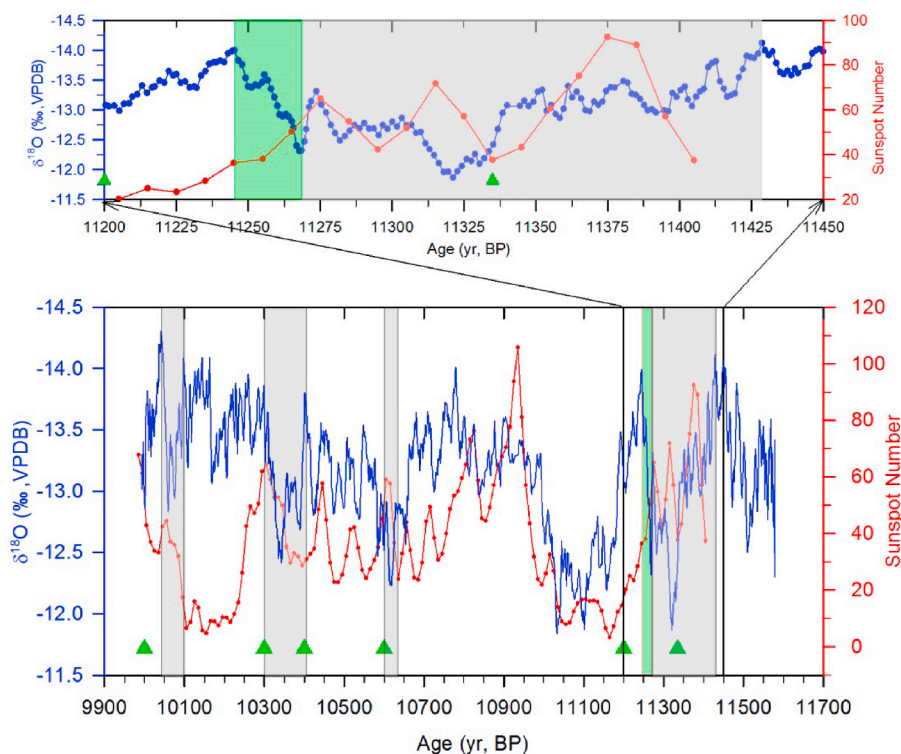


Fig. 6. Comparison of the ZJG-1 $\delta^{18}\text{O}$ records (the blue line and cycles are a 5-point running average) with sunspot number data (Solanki et al., 2004). In the lower panel, the green triangles indicate the occurrence of the freshwater outburst events (Fisher et al., 2002; Teller et al., 2002) and the vertical gray bars show the abrupt climate changes related to the freshwater outbursts. In the upper panel, the vertical gray bar shows the PBO event, and the green bar illustrates the rapid warming event after the PBO event.

abrupt warming event. We suggest that the conditions of AMOC after the PBO event in the early Holocene were similar to those during the D-O events. After the PBO event triggered by the freshwater outburst, persistent freshwater input decreased the salinity in the North Atlantic at 45°N latitude beneath the stadial sea ice lid, and the latitudinal gradient of sea surface salinity continuously increased. Eventually, a critical salinity gradient was exceeded, and a sudden strong northward flux of warm salinity Atlantic water occurred. This caused a transition to warm interstadial conditions and the rapid warming event after the PBO occurred (Peltier and Vettoretti, 2014).

5.4. Spectral analysis

Spectral analysis of proxy records is a powerful tool to analyze the cyclic variation of a time series. To extract the cyclical variation in our records, spectral analysis was performed on the $\delta^{18}\text{O}$ record of travertine profile ZJG-1 using the REDFIT program for unevenly spaced time-series (Schulz and Mudelsee, 2002). The results show a statistically significant peak (above the 99% confidence level) at 226-year, and peaks at 132, 88, 65, 61, 8.9, and 7.6 years are also notable (above the 90% confidence level) (Fig. 7).

The cycles observed in our data at 226, 132, 88 and 61 years were also reported in the $\Delta^{14}\text{C}$ record (Stuiver and Braziunas, 1993) and other climate records from the ASM domain area (Neff et al., 2001; Agnihotri et al., 2002; Fleitmann et al., 2003; Dykoski et al., 2005; Gupta et al., 2005; Cai et al., 2012). The periodicities observed in our data at 226 and 132 years closely match the periodicities of sunspot numbers (226, 132 years) (Gupta et al., 2005), indicating a century-scale relation between solar and ASM intensity. The observed 88-year cycle may correspond to the Gleissberg cycle of solar origin. The cycle observed in our data at 8.9 years was also reported in the record from the ASM domain area (Neff et al., 2001). The 8.9-year cycle is close to the 10.4-year periodicity of the tree-ring $\Delta^{14}\text{C}$ record, which has been assigned to solar modulation (Stuiver and Braziunas, 1993). These spectral results further support the earlier suggestion that solar forcing was responsible for ASM intensity changes during the early Holocene (Fleitmann et al., 2003; Wang et al.,

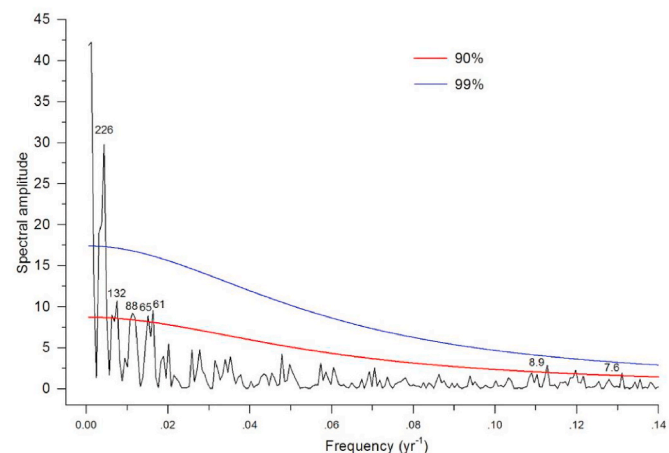


Fig. 7. Spectral analysis results of the ZJG-1 $\delta^{18}\text{O}$ time series. Blue and red lines represent the 99% and 90% significance levels, respectively. The results were obtained using the REDFIT spectral analysis program for unevenly spaced paleoclimate data (Schulz and Mudelsee, 2002).

2005).

6. Conclusions

The cause of decadal to centennial time scales abrupt ASM changes is still debated. Based on the absolute ^{230}Th dating and high-resolution oxygen isotope analysis, we establish a travertine $\delta^{18}\text{O}$ records spanning from 11.6 to 10.0 ka BP, covering the Preboreal Oscillation in the early Holocene, with a temporal resolution of 0.9–2 years. Our record shows that the $\delta^{18}\text{O}$ record of travertine ZJG-1 primarily reflect the changes in Asian Summer Monsoon intensity. On decadal timescales, the changes of the ASM intensity are correlated with solar activity, supporting the notion that changes in solar activity is the primary driving force of the ASM intensity on decadal timescales in the early Holocene.

The PBO event was triggered by the freshwater outburst, but the variations of ASM intensity on decadal timescales during the PBO event were controlled by the interaction of solar activity and the freshwater outburst. The rapid warming event after PBO is similar to the warming events in the D-O events, and may be controlled by the same mechanism. Spectrum analysis results reveal significant peaks at the frequencies typical of solar activity cycles, implying that the solar activity plays the dominated role in driving changes in the ASM intensity.

Declaration of competing interest

The authors declare that they have no known competing financial interests or personal relationships that could have appeared to influence the work reported in this paper.

Acknowledgments

This work was supported by the National Natural Science Foundation of China (Grant Nos. 41372263 and 41977298), the Strategic Priority Research Program of Chinese Academy of Sciences (Grant No. XDB40000000), the Scientific Research and Technology Development Program of Guangxi Zhuang Autonomous Region, China (AB21196050), Guizhou Provincial 2019 Science and Technology Subsidies (No. GZ2019SIG). Special thanks are given to Prof. Dr. Zaihua Liu for his funding support, his thoughtful comments and corrections, which greatly improved the original draft. We also thank Dr. Jinliu Zhang, Prof. Xiuyang Jiang for their assistance in field and laboratory. U-Th dating was provided by grants from the Science Vanguard Research Program of the Ministry of Science and Technology (MOST) (110-2123-M-002-009), the National Taiwan University (110L8907 to C.-C.S.), and the Higher Education Sprout Project of the Ministry of Education (110L901001 and 110L8907). We thank LetPub (www letpub com) for linguistic assistance and pre-submission expert review.

References

- An, Z., Porter, S.C., Kutzbach, J.E., Wu, X., Wang, S., Liu, X., Li, X., Zhou, W., 2000. Asynchronous Holocene optimum of the east asian monsoon. *Quat. Sci. Rev.* 19, 743–762.
- Agnihotri, R., Dutta, K., Bhushan, R., Somayajulu, B.L.K., 2002. Evidence for solar forcing on the Indian monsoon during the last millennium. *Earth Planet Sci. Lett.* 198, 521–527.
- Ayalon, A., Bar-Matthews, M., Sass, E., 1998. Rainfall-recharge relationships within a karstic terrain in the eastern Mediterranean semi-arid region, Israel: $\delta^{18}\text{O}$ and 8D characteristics. *J. Hydrol.* 207, 18–31.
- Berkelhammer, M., Sinha, A., Stott, L., Cheng, H., Pausata, F., Yoshimura, K., 2012. An abrupt shift in the Indian Monsoon 4,000 years ago. In: Giosan, L., Fuller, D.Q., Nicoll, K.R., Flad, K., Clift, P.D. (Eds.), *Geophysical Monograph Series: Climate Landscapes and Civilization*. American Geophysical Union, Washington, D.C., pp. 75–88.
- Berner, K.S., Koc, N., Godtliebsen, F., 2010. High frequency climate variability of the Norwegian Atlantic Current during the early Holocene period and a possible connection to the Gleissberg cycle. *Holocene* 20, 245–255.
- Björck, S., Kromer, B., Johnsen, S., Bennike, O., Hammarlund, D., Lemdahl, G., Possnert, G., Rasmussen, T.L., Wohlfarth, B., Hammer, C.U., Spurk, M., 1996. Synchronized terrestrial-atmospheric deglacial records around the North Atlantic. *Science* 274 (5290), 1155–1160.
- Bird, B.W., Polisar, P.J., Lei, Y., Thompson, L.G., Yao, T., Finney, B.P., Bain, D.J., Pompeani, D.P., Strinman, B.A., 2014. A Tibetan lake sediment record of Holocene Indian summer monsoon variability. *Earth Planet Sci. Lett.* 399, 92–102.
- Bond, G., Showers, W., Cheseby, M., Lotti, R., Almasi, P., DeMenocal, P., Priore, P., Cullen, H., Hajdas, I., Bonani, G., 1997. A pervasive millennial-scale cycle in North Atlantic Holocene and glacial climates. *Science* 278, 1257–1266.
- Bond, G., Kromer, B., Beer, J., Muscheler, R., Evans, M.N., Showers, W., Hoffmann, S., Lotti-Bond, R., Hajdas, I., Bonani, G., 2001. Persistent solar influence on North Atlantic climate during the Holocene. *Science* 294, 2130–2136.
- Brasier, A.T., Andrews, J.E., Marca-Bell, A.D., Dennis, P.F., 2010. Depositional continuity of seasonally laminated tufas: implications for $\delta^{18}\text{O}$ based palaeotemperatures. *Global Planet. Change* 71, 160–167.
- Cai, Y., Tan, L., Cheng, H., An, Z., Edwards, R.L., Kelly, M.J., Kong, X., Wang, X., 2010. The variation of summer monsoon precipitation in central China since the last deglaciation. *Earth Planet Sci. Lett.* 291, 0–31.
- Cai, Y., Zhang, H., Cheng, H., An, Z., Edwards, R.L., Wang, X., Tan, L., Liang, F., Wang, J., Kelly, M., 2012. The Holocene Indian monsoon variability over the southern Tibetan Plateau and its teleconnections. *Earth Planet Sci. Lett.* 335–336, 135–144.
- Breitenbach, S.F.M., Rehfeld, K., Goswami, B., Baldini, J.U.L., Ridley, H.E., Kennett, D.J., Pruffer, K.M., Aquino, V.V., Asmerom, Y., Polyak, V.J., Cheng, H., Kurths, J., Marwan, N., 2012. Constructing proxy records from age models (COPRA). *Clim. Past* 8, 1765–1779.
- Cai, Y., Fung, I.Y., Edward, R.L., An, Z., 2015. Variability of stalagmite-inferred Indian monsoon precipitation over the past 252,000 y. *Proc. Natl. Acad. Sci. U. S. A.* 112 (10), 2954–2959.
- Cheng, H., Fleitmann, D., Edwards, R.L., Wang, X., Cruz, F.W., Auler, A.S., Mangini, A., Wang, Y., Kong, X., Burns, S.J., Matter, A., 2011. Timing and structure of the 8.2 kyr B.P. event inferred from $\delta^{18}\text{O}$ records of stalagmites from China, Oman, and Brazil. *Geology* 37, 1007–1010.
- Cheng, H., Edwards, R.L., Shen, C.-C., Polyak, V.J., Asmerom, Y., Woodhead, J., Hellstrom, J., Wang, Y., Kong, X., Spötl, C., Wang, X., Alexander Jr., E.C., 2013. Improvements in ^{230}Th dating, ^{230}Th and ^{234}U half-life values, and U-Th isotopic measurements by multi-collector inductively coupled plasma mass spectrometry. *Earth Planet Sci. Lett.* 371–372, 82–91.
- Clement, A.C., Peterson, L.C., 2008. Mechanisms of abrupt climate change of the last glacial period. *Rev. Geophys.* 46, RG4002.
- Dansgaard, W., 1964. Stable isotopes in precipitation. *Tellus* 16, 436–468.
- Dansgaard, W., Johnsen, S.J., Clausen, H.B., Dahl-Jensen, D., Gundestrup, N.S., Hammer, C.U., Hvidberg, C.S., Steffensen, J.P., Sveinbjörnsdóttir, A.E., Jouzel, J., Bond, G., 1993. Evidence for general instability of past climate from a 250-kyr ice-core record. *Nature* 364, 218–220.
- Dokken, T.M., Nisancioglu, K.H., Li, C., Battisti, D.S., Kissel, C., 2013. Dansgaard-Oeschger cycles: interactions between ocean and sea ice intrinsic to the Nordic Seas. *Paleoceanography* 28, 491–502.
- Dong, J., Wang, Y., Cheng, H., Hardt, B., Edwards, R.L., Kong, X., Wu, J., Chen, S., Liu, D., Jiang, X., Zhao, K., 2010. A high-resolution stalagmite record of the Holocene East Asian monsoon from Mt Shennongjia, central China. *Holocene* 20 (2), 257–264.
- Dorale, J.A., Liu, Z., 2009. Limitations of Hendy test criteria in judging the paleoclimatic suitability of speleothems and the need for replication. *J. Cave Karst Stud.* 71, 73–80.
- Dykoski, C.A., Edwards, R.L., Cheng, H., Yuan, D., Cai, Y., Zhang, M., Lin, Y., Qing, J., An, Z., Revenaugh, J., 2005. A high-resolution, absolute-dated Holocene and deglacial Asian monsoon record from Dongge Cave, China. *Earth Planet Sci. Lett.* 233, 71–86.
- Elliot, M.L., Labeyrie, L., Duplessy, J.C., 2002. Changes in North Atlantic deep-water formation associated with the Dansgaard-Oeschger temperature oscillations (60–10ka). *Quat. Sci. Rev.* 21, 1153–1165.
- Fisher, T.G., Smith, D.G., Andrews, J.T., 2002. Preboreal oscillation caused by a glacial Lake Agassiz flood. *Quat. Sci. Rev.* 21, 873–878.
- Fleitmann, D., Burns, S.J., Mudelsee, M., Neff, U., Kramers, J., Mangini, A., Matter, A., 2003. Holocene forcing of the Indian Monsoon recorded in a stalagmite from southern Oman. *Science* 300, 1737–1739.
- Fleitmann, D., Burns, S.J., Mangini, A., Mudelsee, M., Kramers, J., Villa, I., Neff, U., Al-Sabbari, A.A., Buetner, A., Hippler, A., Matter, A., 2007. Holocene ITCZ and Indian monsoon dynamics recorded in stalagmites from Oman and Yemen (Socotra). *Quat. Sci. Rev.* 26, 170–188.
- Fleitmann, D., Mudelsee, M., Burns, S.J., Bradley, R.S., Kramers, J., Matter, A., 2008. Evidence for a widespread climatic anomaly at around 9.2 ka before present. *Paleoceanography* 23, PA1102.
- Ford, T.D., Pedley, H.M., 1996. A review of tufa and travertine deposits of the world. *Earth Sci. Rev.* 41, 117–175.
- Ganopolski, A., Rahmstorf, S., 2001. Rapid changes of glacial climate simulated in a coupled climate model. *Nature* 409, 153–158.
- Gupta, A.K., Anderson, D.M., Overpeck, J.T., 2003. Abrupt changes in the asian southwest monsoon during the Holocene and their links to the North Atlantic Ocean. *Nature* 421, 354–357.
- Gupta, A.K., Das, M., Anderson, D.M., 2005. Solar influence on the Indian summer monsoon during the Holocene. *Geophys. Res. Lett.* 32, L17703.
- Gupta, A.K., Mohan, K., Das, M., Singh, R., 2013. Solar forcing of the Indian summer monsoon variability during the Allerød period. *Sci. Rep.* 3, 2753.
- Haug, G.H., Hughen, K.A., Sigman, D.M., Peterson, L.C., Röhrl, U., 2001. Southward migration of the intertropical convergence zone through the Holocene. *Science* 293, 1304–1308.
- Hong, Y., Hong, B., Lin, Q., Zhu, Y., Shibata, Y., Hirota, M., Uchida, M., Leng, X., Jiang, H., Xu, H., Wang, H., Yi, L., 2003. Correlation between Indian ocean summer monsoon and North Atlantic climate during the Holocene. *Earth Planet Sci. Lett.* 211, 371–380.
- Hori, M., Hoshino, K., Okumura, K., Kano, A., 2008. Seasonal patterns of carbon chemistry and isotopes in tufa depositing groundwaters of southwestern Japan. *Geochim. Cosmochim. Acta* 72, 480–492.
- Jaffey, A.H., Flynn, K.F., Glendenin, L.E., Bentley, W.C., Essling, A.M., 1971. Precision measurement of half-lives and specific activities of ^{235}U and ^{238}U . *Phys. Rev. C* 4, 1889–1906.
- Kano, A., Hagiwara, R., Kawai, T., Hori, M., Matsuoka, J., 2007. Climatic conditions and hydrological change recorded in a high-resolution stable-isotope profile of a recent laminated tufa on a subtropical island, southern Japan. *J. Sediment. Res.* 77, 59–67.
- Kobashi, T., Severinghaus, J.P., Barnola, J.M., 2008. $4 \pm 1.5^\circ\text{C}$ abrupt warming 11,270 yr ago identified from trapped air in Greenland ice. *Earth Planet Sci. Lett.* 268 (3–4), 397–407.
- Kodera, K., 2004. Solar influence on the Indian Ocean monsoon through dynamical processes. *Geophys. Res. Lett.* 31, L24209.
- Liu, D., Wang, Y., Cheng, H., Edwards, R.L., Kong, X., Chen, S., Liu, S., 2018. Contrasting patterns in abrupt Asian summer monsoon changes in the last glacial period and the Holocene. *Paleoceanogr. Paleoclimatol.* 33, 214–226.

- Liu, X., Chen, B., 2000. Climatic warming in the Tibetan Plateau during recent decades. *Int. J. Climatol.* 20, 1729–1742.
- Liu, Z., Svensson, U., Dreybrodt, W., Yuan, D., Buhmann, D., 1995. Hydrodynamic control of inorganic calcite precipitation in Huanglong Ravine, China: field measurements and theoretical prediction of deposition rates. *Geochem. Cosmochim. Acta* 59, 3087–3097.
- Liu, Z., Zhang, M., Li, Q., You, S., 2003. Hydrochemical and isotope characteristic of spring water and travertine in the Baishuitai area (SW China) and their meaning for paleoenvironmental reconstruction. *Environ. Geol.* 44, 698–704.
- Liu, Z., Li, H., You, C., Wan, N., Sun, H., 2006. Thickness and stable isotopic characteristics of modern seasonal climate-controlled sub-annual travertine laminas in a travertine-depositing stream at Baishuitai, SW China: implications for paleoclimate reconstruction. *Environ. Geol.* 51, 257–265.
- Liu, Z., Sun, H., Lu, B., Liu, X., Ye, W., Zeng, C., 2010. Wet-dry seasonal variations of hydrochemistry and carbonate deposition rates in a travertine-depositing canal at Baishuitai, Yunnan, SW China: implications for the formation of biannual laminae in travertine and for climatic reconstruction. *Chem. Geol.* 273, 258–266.
- Lojen, S., Trkov, A., Šćančar, J., Vázquez-Navarro, J.A., Cukrov, N., 2009. Continuous 60-year stable isotopic and earth-alkal element records in a modern laminated tufa (Jaruga, river Krka, Croatia): implications for climate reconstruction. *Chem. Geol.* 258, 242–250.
- Luo, H., Yanai, M., 1984. The large-scale circulation and heat source over the Tibetan Plateau and surrounding areas during the early summer of 1979. Part II: heat and moisture budgets. *Mon. Weather Rev.* 112, 966–989.
- Matsuoka, J., Kano, A., Oba, T., Watanabe, T., Sakai, S., Seto, K., 2001. Seasonal variation of stable isotopic compositions recorded in a laminated tufa, SW Japan. *Earth Planet Sci. Lett.* 192, 31–44.
- Magny, M., Vannière, B., Beaulieu, J., Bégeot, C., Heiri, O., Millet, L., Peyron, O., Walter-Simonnet, A., 2007. Early-Holocene climatic oscillations recorded by lake-level fluctuations in west-central Europe and in central Italy. *Quat. Sci. Rev.* 26 (15–16), 1951–1964.
- Neff, U., Burns, S.J., Mangini, A., Mudelsee, M., Fleitmann, D., 2001. Strong coherence between solar variability and monsoon in Oman between 9 and 6 kyr ago. *Nature* 411, 290–293.
- Nesje, A., Dahl, S.O., Bakke, J., 2004. Were abrupt Lateglacial and early-Holocene climatic changes in northwest Europe linked to freshwater outbursts to the North Atlantic and Arctic Oceans? *Holocene* 14, 299–310.
- O'Neil, J.R., Clayton, R.N., Mayeda, T.K., 1969. Oxygen isotope fractionation in divalent metal carbonates. *J. Chem. Phys.* 51, 5547–5558.
- Orland, I.J., Burstyn, Y., Bar-Matthews, M., Kozdon, R., Ayalon, A., Matthews, A., Valley, J.W., 2014. Seasonal climate signals (1990–2008) in a modern Soreq Cave stalagmite as revealed by high-resolution geochemical analysis. *Chem. Geol.* 363, 322–333.
- Park, H.S., Chiang, J., Bordoni, S., 2012. The mechanical impact of the Tibetan Plateau on the seasonal evolution of the South Asian Monsoon. *J. Clim.* 25, 2394–2407.
- Peltier, W.R., Vettoretti, G., 2014. Dansgaard-Oeschger oscillations predicted in a comprehensive model of glacial climate: a “kicked” salt oscillator in the Atlantic. *Geophys. Res. Lett.* 41, 7306–7313.
- Pentecost, A., 1995. The quaternary travertine deposits of europe and asia minor. *Quat. Sci. Rev.* 14, 1005–1028.
- Rasmussen, S.O., Vinther, B.M., Clausen, H.B., Andersen, K.K., 2007. Early Holocene climate oscillations recorded in three Greenland ice cores. *Quat. Sci. Rev.* 26, 1907–1914.
- Rozanski, K., Araguas-Araguas, L., Gonfiantini, R., 1992. Relation between long-term trends of Oxygen-18 isotope composition of precipitation and climate. *Science* 258, 981–985.
- Sato, T., Kimura, F., 2005. Impact of diabatic heating over the Tibetan Plateau on subsidence over northeast Asian arid region. *Geophys. Res. Lett.* 32, L05809.
- Schulz, M., Mudelsee, M., 2002. REDFIT: estimating red-noise spectra directly from unevenly spaced paleoclimatic time series. *Comput. Geosci.* 28, 421–426.
- Shen, C.-C., Cheng, H., Edwards, R.L., Moran, S.B., Edmonds, H.N., Hoff, J.A., Thomas, R.B., 2003. Measurement of attogram quantities of ^{231}Pa in dissolved and particulate fractions of seawater by isotope dilution thermal ionization mass spectroscopy. *Anal. Chem.* 75, 1075–1079.
- Shen, C.-C., Edwards, R.L., Cheng, H., Dorale, J.A., Thomas, R.B., Moran, S.B., Weinstein, S.E., Edmonds, H.N., 2002. Uranium and thorium isotopic and concentration measurements by magnetic sector inductively coupled plasma mass spectrometry. *Chem. Geol.* 185, 165–178.
- Shen, C.-C., Wu, C.-C., Cheng, H., Edwards, R., Hsieh, Y., Gallet, S., Chang, C., Li, T., Lam, D., Kano, A., Horl, M., Spötl, C., 2012. High-precision and high-resolution carbonate ^{230}Th dating by MC-ICP-MS with SEM protocols. *Geochem. Cosmochim. Acta* 99, 71–86.
- Solanki, S., Usoskin, I., Kromer, B., Schüssler, M., Beer, J., 2004. Unusual activity of the Sun during recent decades compared to the previous 11,000 years. *Nature* 431, 1084–1087.
- Stuiver, M., Braziunas, T.F., 1993. Sun, ocean, climate and atmospheric $^{14}\text{CO}_2$: an evaluation of causal and spectral relationships. *Holocene* 3, 289–305.
- Stuiver, M., Braziunas, T.F., Grootes, P.M., Zielinski, G.A., 1997. Is there evidence for solar forcing of climate in the GISP2 oxygen isotope record? *Quat. Res.* 48, 259–266.
- Sun, H., Liu, Z., 2010. Wet-dry seasonal and spatial variations in the $\delta^{13}\text{C}$ and $\delta^{18}\text{O}$ values of the modern endogenic travertine at Baishuitai, Yunnan, SW China and their paleoclimatic and paleoenvironmental implications. *Geochem. Cosmochim. Acta* 74, 1016–1029.
- Sun, W., Zhang, E., Liu, E., Ji, M., Chen, R., Zhao, C., Shen, J., Li, Y., 2017. Oscillations in the Indian summer monsoon during the Holocene inferred from a stable isotope record from pyrogenic carbon from lake Chenghai, southwest China. *J. Asian Earth Sci.* 134, 29–36.
- Sun, W., Zhang, E., Shulmeister, J., Bird, M.I., Chang, J., Shen, J., 2019. Abrupt changes in Indian summer monsoon strength during the last deglaciation and early Holocene based on stable isotope evidence from Lake Chenghai, southwest China. *Quat. Sci. Rev.* 218, 1–9.
- Teller, J.T., Leverington, D.W., Mann, J.D., 2002. Freshwater outbursts to the oceans from glacial Lake Agassiz and their role in climate change during the last deglaciation. *Quat. Sci. Rev.* 21, 879–887.
- van der Plicht, J., van Geel, B., Bohncke, S.J.P., Bos, J.A.A., Blaauw, M., Speranza, A.O. M., Muscheler, R., Björck, S., 2004. The Preboreal climate reversal and a subsequent solar-forced climate shift. *J. Quat. Sci.* 19, 263–269.
- van Kreveld, S., Sarnthein, M., Erlenerker, H., Grootes, P., Jung, S., Nadeau, M.J., Pflaumann, U., Voelker, A., 2000. Potential links between surging ice sheets, circulation changes, and the Dansgaard-Oeschger cycles in the Irminger Sea, 60–18 kyr. *Paleoceanography* 15, 425–442.
- Wang, Y., Cheng, H., Edwards, R.L., He, Y., Kong, X., An, Z., Wu, J., Kelly, M.J., Dykoski, C.A., Li, X., 2005. The Holocene asian monsoon: links to solar changes and North Atlantic climate. *Science* 308, 854–857.
- Wang, H., Liu, Z., Zhang, J., Sun, H., An, D., Fu, R., Wang, X., 2010. Spatial and temporal hydrochemical variation of the spring-fed travertine-deposition stream in the Huanglong Ravine, Sichuan SW China. *Acta Carsol.* 39, 247–259.
- Wang, H., Yan, H., Liu, Z., 2014. Contrasts in variations of the carbon and oxygen isotopic composition of travertines formed in pools and a ramp stream at Huanglong Ravine, China: implications for paleoclimatic interpretations. *Geochem. Cosmochim. Acta* 125, 34–38.
- Wang, Y., Zhang, E., Sun, W., Chang, J., Liu, X., Ni, Z., Ning, D., 2019. Holocene evolution of the Indian summer monsoon inferred from a lacustrine record of lake wuxu, south-east Tibetan plateau. *J. Quat. Sci.* 34, 1–12.
- Wu, G.X., Zhang, Y.S., 1998. Tibetan plateau forcing and the timing of the monsoon onset over south asia and the south China sea. *Mon. Weather Rev.* 126, 913–927.
- Xu, H., Yeager, K.M., Lan, J., Liu, B., Sheng, E., Zhou, X., 2015. Abrupt Holocene Indian Summer Monsoon failures: a primary response to solar activity? *Holocene* 25, 677–685.
- Yan, H., Sun, H., Liu, Z., 2012. Equilibrium vs. kinetic fractionation of oxygen isotopes in two low-temperature travertine-depositing systems with differing hydrodynamic conditions at Baishuitai, Yunnan, SW China. *Geochem. Cosmochim. Acta* 95, 63–78.
- Yan, H., Liu, Z., Sun, H., 2017. Effect of in-stream physicochemical processes on the seasonal variations in $\delta^{13}\text{C}$ and $\delta^{18}\text{O}$ values in laminated travertine deposits in a mountain stream channel. *Geochem. Cosmochim. Acta* 202, 179–189.
- Yang, X., Zhang, P., Chen, F., Huh, C., Li, H., Cheng, H., Kathleen, R., Liu, J., An, C., 2007. Modern stalagmite oxygen isotopic composition and its implications of climatic change from a high-elevation cave in the eastern Qinghai-Tibet Plateau over the past 50 years. *Chin. Sci. Bull.* 52, 1238–1247.
- Yang, Y., Yuan, D., Cheng, H., Zhang, M., Qin, J., Lin, Y., Zhu, X., Edwards, R.L., 2010. Precise dating of abrupt shifts in the Asian Monsoon during the last deglaciation based on stalagmite data from Yamen Cave, Guizhou Province, China. *Sci. Chin. (Series D)* 53, 633–641.
- Yeh, T.C., Luo, S.W., Chu, P.C., 1957. The wind structure and heat balance in the lower troposphere over Tibetan Plateau and its surrounding. *Acta Meteorol. Sin.* 28, 108–121.
- Zeng, M., Zhu, C., Song, Y., Ma, C., Yang, Z., 2017. Paleoenvironment change and its impact on carbon and nitrogen accumulation in the Zoige wetland, northeastern Qinghai-Tibetan Plateau over the past 14,000 years. *G-cubed* 18, 1775–1792.
- Zhang, E., Sun, W., Chang, J., Ning, D., Shulmeister, J., 2018. Variations of the Indian summer monsoon over the last 30 000 years inferred from a pyrogenic carbon record from south-west China. *J. Quat. Sci.* 33 (1), 131–138.
- Zhang, H., Yin, J., Cheng, H., Edwards, R.L., Lin, Y., Tang, W., Yang, H., Tu, L., Wang, H., Pan, M., Wu, X., 2016. Discussion about the mechanism of the weak summer monsoon events during the early Holocene: a case study of precisely dated stalagmite record from Lianhua cave, Hunan province, China. *Acta Sedimentol. Sin.* 34, 281–291 (In English Abstract).
- Zhao, Y., Yu, Z., Zhao, W., 2011. Holocene vegetation and climate histories in the eastern Tibetan Plateau: controls by insolation-driven temperature or monsoon-derived precipitation changes? *Quat. Sci. Rev.* 30, 1173–1184.
- Zhou, W., Yu, S.Y., Burr, G.S., Kukla, G.J., Jull, A.J.T., Xian, F., Xiao, J., Colman, S.M., Yu, H., Liu, Z., Kong, X., 2010. Postglacial changes in the Asian summer monsoon system: a pollen record from the eastern margin of the Tibetan Plateau. *Boreas* 39, 528–539.